Applied Surface Science 319 (2014) 211–215

Contents lists available at ScienceDirect

Applied Surface Science

journal homepage: www.elsevier.com/locate/apsusc

One-step synthesis of bird cage-like ZnO and other controlled morphologies: Structural, growth mechanism and photocatalytic properties

Shuo Yang[a,b], Jian Wang[a,b,c], Xiuyan Li[c], Hongju Zhai[c], Donglai Han[a,b,c], Bing Wei[c], Dandan Wang[a,b,c], Jinghai Yang[a,c,*]

[a] Changchun Institute of Optics, Fine Mechanics and Physics, Chinese Academy of Sciences, Changchun 130033, P.R. China
[b] University of Chinese Academy of Sciences, Beijing 100049, P.R. China
[c] Key Laboratory of Functional Materials Physics and Chemistry (Jilin Normal University), Ministry of Education, Siping 136000, P.R. China

ARTICLE INFO

Article history:
Received 27 May 2014
Received in revised form 25 July 2014
Accepted 26 July 2014
Available online 4 August 2014

Keywords:
ZnO
Morphology control
Growth mechanism
Photocatalytic

ABSTRACT

ZnO nanocages and other nanostructures have been synthesized via a simple one-pot hydrothermal method with different reaction times. It is worth mentioning that this is a completely green method which does not require any other chemicals except that Zn foil served as Zn source in the experiment. X-ray diffraction (XRD), Scanning electron microscopy (SEM), transmission electron microscopy (TEM), photoluminescence (PL) and UV–Vis diffuse reflection spectra were used to characterize the crystallinity, morphology and optical property of ZnO structures. Growth mechanisms of ZnO were proposed based on these results. Furthermore, ZnO films with different morphologies and crystal growth habits exhibited different activities to rhodamine B degradation. The influence of the reaction time on the morphology of ZnO films and the effect of the morphologies on the photocatalytic activity are discussed.

1. Introduction

After World War II, environmental problems are increasing day by day accompanied with the world population's explosive growth. The pollution was so serious that it was far beyond the environment's self-cleaning ability in some densely populated areas [1–4]. So the key point in environmental management is controlling and eliminating chemical contaminants which will bring threat to water resource, soil and atmospheric environment. The crux in environmental conservation is to explore a new technique to eliminate chemical contaminants. Physical absorption [5], chemical oxidation [6], microbial treatment [7] and burning method are typical pollution treatment methods; they have made great contribution to the protection of environment [8]. But in these methods exist many disadvantages, for example, low efficiency, high energy consumption. Furthermore, they cannot eliminate chemical contaminants completely and so on [9]. Thus, the pursued target of environmental protection technology is to explore high efficiency, low energy consumption, wide using range and deep oxidation ability to degrade chemical pollutants.

Photocatalysis technology is a new environmental protection technology developed since the 1970s in this background [10,11]. Because the surface of semiconductor materials can be excited under illumination, it can be used to degrade organics [12,13], restore heavy metal iron [14], kill bacteria [15] and eliminate peculiar smell [16,17] by using optical energy in room temperature. ZnO photocatalyst is non-toxic and it can be applied to eliminate organic pollutants from waste water [18–21]. But the form of ZnO photocatalyst also has strong influences on the photocatalytic activity. Micro/nanosized catalyst powders exhibited high solid to liquid contact areas which helped to achieve high reaction rates in waste water handling [22–24]. So ZnO photocatalysts are often applied in the form of powders. However, many specific questions emerge including the particle aggregation, together with the need for the separation and recycling of the photocatalyst nanoparticles from the slurry after the wastewater treatment process. Recent investigations on photocatalysis are oriented toward the immobilization of photocatalyst as thin films on the support substrates [25,26].

In this paper, we reported a novel chemical method to synthesize ZnO films using a green, simple and low-temperature hydrothermal method. Also, it does not require any templates, catalysts or even other chemicals except Zn foil serve as Zn source. The optical properties and the photocatalytic efficiency on decomposition rhodamine B (RhB) were also explored.

* Corresponding author. Tel./fax: +86 434 3294566.
E-mail address: jhyang1@jlnu.edu.cn (J. Yang).

http://dx.doi.org/10.1016/j.apsusc.2014.07.165
0169-4332/

2. Experimental

2.1. Materials

All reagents, including Zn foil, ethanol and rhodamine B (RhB), were of analytical grade, purchased from Sinopharm Chemical Regent Co., Ltd, and used without further purification.

2.2. Preparation

The synthesis process of ZnO nano arrays contains only one step-hydrothermal growth. Preparation does not need any other chemical reagent except Zn foils, which serve as Zn source and growth substrates. Zn foils were ultrasonically cleaned with ethanol and deionized water for several times before experiment, respectively. Several milliliters deionized water was injected into Telfon-lined stainless steel autoclaves. Then Zn substrates were transferred to Telfon-lined stainless steel autoclaves heated at 100 °C for different time. After growth, the substrates were washed with deionized water and ethanol, and then dried at room temperature.

2.3. Characterization

The crystal structures of ZnO films were measured by X-ray power diffraction (XRD) pattern using a D/max-RA XRD diffraction spectrometer (MAC Science, MXP18, Japan) with a Cu Kα line at 1.5406 Å. The morphologies and structures of films were observed by scanning electron microscope (SEM, Hitachi, S-570) and transition electron microscopy (TEM, JEOL JEM-2010HR). The photoluminescence (PL) spectra were measured at room temperature using a He-Cd laser with a wavelength of 325 nm as the excitation source. UV–Vis Diffuse reflection spectra (UV-DRS) of the samples were recorded on a Lambda-900 spectrophotometer, and $BaSO_4$ was used as a reference.

2.4. Photocatalysis

For photocatalytic activity studies, films with the same geometric area (1 cm × 1 cm) were settled in a 4.5 mL RhB aqueous solution with a concentration of 7 mg/L in a glass cell, and the ultraviolet light was provided by a high-pressure Hg lamp (main wavelength: 365 nm). Prior to irradiation, the films were immersed in the same solution for 0.5 h in darkness to establish adsorption equilibrium. The residual concentration of RhB after irradiation for a definite time was estimated according to the absorbance at 555 nm measured by UV–Vis spectrophotometer (UV-5800PC, Shanghai Metash Instruments Co., Ltd).

3. Results and discussion

3.1. Morphology and structure

The crystal phase and phase purity of ZnO films were examined by XRD. XRD pattern of pure zinc foil before chemical reaction is given in Fig. 1 (a) to make the comparison easy. All of peaks in Fig. 1 (a) can be indexed to Zn (JCPDS No. 04-0831) and no impurity peaks were found in the pattern. According to Fig. 1 (b)–(e), new peaks which can be indexed to wurtzite ZnO with hexagonal wurtzite structure (JCPDS 36-1451) appeared more clearly with the extended reaction time. The peaks indicated that these ZnO crystals grow on Zn substrates are in high crystallinity. No other impurity peaks were found in the all patterns.

The growth processes of nanostructures on the Zn foil substrate were examined in detail by SEM. Fig. 2(a)–(d) shows the SEM images of the as-prepared ZnO films grown on Zn substrates within

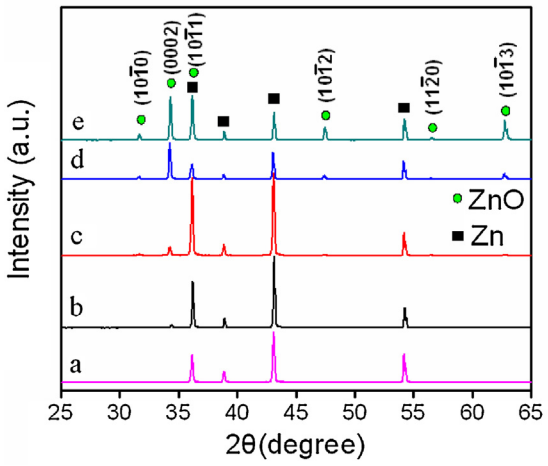

Fig. 1. XRD patterns of ZnO films for different deposition time. (a) Pure Zinc foil before chemical reaction, (b) 5 h, (c) 1 d, (d) 2 d and (e) 3 d.

5 h to 3days, and the corresponding films were defined as films of 1#–4#, respectively. For ZnO film 1# with 5 h of hydrothermal growth, there were only a layer of tiny granules formed. Through comparison between Fig. 2(a) and its inset image we can confirm those granules are ZnO particles. A subsequent increase in the

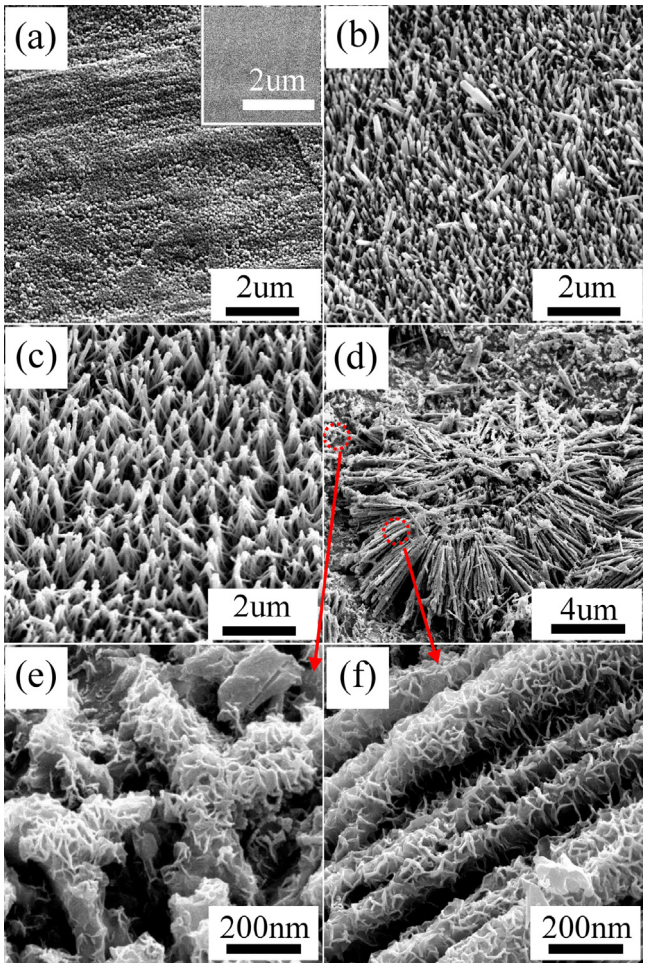

Fig. 2. SEM images of the as-synthesized ZnO nanostructure on the top surface of the Zn foil substrate with different reaction time. (a) 5 h; (b) 1 d; (c) 2 d and (d) 3 d. (e) and (f) are the corresponding high magnification SEM images for Fig. 2d. The inset image in (a) is the morphology of Zn foil before chemical reaction.

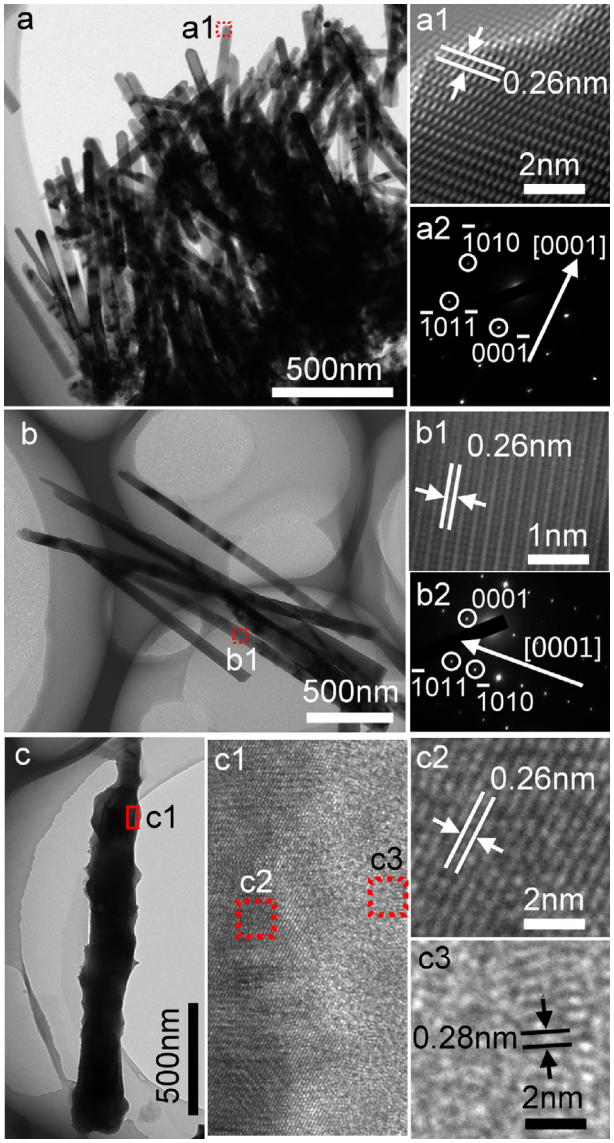

Fig. 3. (a) TEM image of the as-synthesized ZnO nanostructures with different reaction time (a) 1 d; (b) 2 d; (c) 3 d. (a1), (b1), (c1), (c2) and (c3) are the corresponding HRTEM images. (a2) and (b2) are SEAD patterns corresponding to the marked frame areas in (a) and (b), recorded along the [2$\bar{1}\bar{1}$0] zone).

reaction time to 1 d leads to ZnO nanorods with sizes of 70–130 nm in diameter appeared on the Zn foil substrate. A further increasing in the reaction time results in an interesting scene. After 2 days of reaction time ZnO nanorods' heads contact tightness like bird cages. Most of bird cages have six or seven bars (ZnO nanorods) with sizes of 80–160 nm in diameter. Some bird cages even have a dozen bars. Finally, when the reaction time reaches 3 d the maize straw-like ZnO with a diameter of 180–220 nm and a length of about 6 μm formed on the Zn foil substrate. As its name suggests, many wrinkles appeared on the surfaces of maize straw-like ZnO nanostructures just like leaves on maize straws.

Further information about the ZnO products is obtained from TEM and HRTEM images associated with SAED pattern in Fig. 3. Fig. 3(a) presents the TEM image of the film 2#. The result shows that ZnO nanorods are around 80 nm in diameter, which is in good coincident with the SEM observation (Fig. 2(b)). A high resolution TEM image (Fig. 3(a1)) and associated SAED pattern (Fig. 3(a2)) taken on an individual ZnO nanorod show the single crystalline nature of the film 2#. The HRTEM image in Fig. 3(a1) shows the distance between adjacent lattice facets is about 0.26 nm, corresponding to the distance between two (0 0 0 1) facets of hexagonal ZnO, indicating that ZnO nanorods grown along the <0 0 0 1> direction (*c*-axis) [27]. The corresponding SAED pattern shown in Fig. 3(a2) confirms the single crystal nature of ZnO nanorods grown along the c-axis.

Fig. 3(b) presents a TEM image of the film 3#. ZnO nanorods are around 120 nm in diameter. HRTEM image and SAED pattern of film 3# given the similar message with film 2#. That means according to HRTEM image Fig. 3(b1) and SAED pattern Fig. 3(b2), we can make a judgment that well-crystallized ZnO nanorods grown along the c-axis.

Fig. 3(c) presents a TEM image of a typical isolated ZnO nanorod obtained after 3 days reaction time. From TEM image, ZnO nanorod is around 200 nm in diameter and there are some sheets appear on the surface of ZnO nanorod. Fig. 3(c1) gives an amplifying image for the select area in Fig. 3(c). It is very clear that there exists a layer of amorphous structure in the surface of ZnO nanorod. HRTEM images for the different select area in Fig. 3(c1) were presented in Fig. 3(c2) and (c3). Fig. 3(c2) shows the selected area form the main trunk of ZnO nanorod, the distance between two fringes is about 0.26 nm, which is close to the d spacing of the (0 0 0 1) plane, indicating that the <0 0 0 1> direction (*c* axis) is the growth direction of ZnO nanorod. But the selected area from the surface of ZnO nanorod Fig. 3(c3) displays a different structure. The distance between two fringes is about 0.28 nm in Fig. 3(c3), which is close to the d spacing of the (1 0 1 0) plane. It indicated that many ZnO quantum dots with uncertain growth orientations spread over the surface of ZnO nanorod.

3.2. Growth mechanism

In accordance with above characterization, a possible growth process of different structures of ZnO was proposed here. In the early stage (after 5 h) of reaction, there formed small ZnO particles on the surface of Zn foil. Because of the structural anisotropy and surface electric polarity of ZnO, the growth rates along crystal direction [0 0 0 1] prior to the other crystal directions. So ZnO nanorods grew along [0 0 0 1] direction spread on the substrate. Because the surface of ZnO foils was not smooth enough to make sure every ZnO rods growth perpendicular to the substrate, ZnO nanorods growth like tripods with their heads contact tightness formed. Along with the extension of reaction process, more and more ZnO rods flock together and lead the formation of ZnO rods heap. After a long enough reaction, ZnO rods will cover most place of the substrate surface. And that would obstruct the release of Zn ion from Zn foil. The corrosion of ZnO rods will be surpassing the growth process and the surface of ZnO rods will be tough after long reaction time (after 3 days).

3.3. Optical properties and photocatalytic activity

The representative PL spectra of as-synthesized ZnO nanostructures with different reaction times are presented in Fig. 4. In general, the room temperature PL spectra of all the as-grown films revealed similar features. There appeared one sharp UV emission band at about 380 nm, generally assigned as a near-band-edge (NBE) emission band, and another broad deep-level emission band extending from 430 to 630 nm. The position of the NBE emission band in our nanostructures agrees well with the reported value [28,29]. ZnO commonly exhibits luminescence in the visible band attribute to different intrinsic or extrinsic defects [30]. The origin of these visible emissions (e.g., green, yellow, orange, and red emissions) is still attracting controversy. For example, a number of different hypotheses have been proposed to explain the green emission, such as a singly ionized oxygen vacancy, V_O center [31,32] an

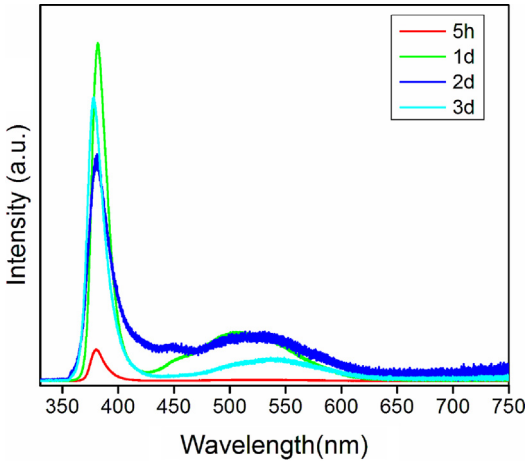

Fig. 4. PL spectra of ZnO films for different deposition time.

oxygen antisites [33], and a zinc vacancy, V_{Zn} [34], etc. Generally, the green emission is typically associated with oxygen deficiency (e.g., excess Zn^{2+} ions or V_O defects), and the yellow/orange emission is attributed to excess oxygen [35–38]. The green transition attributed to the singly ionized oxygen vacancy in ZnO and the emission results from the radiative recombination of a photogenerated hole with an electron occupying the oxygen vacancy. The stronger the relative intensity of the green luminescence is, the more the singly ionized oxygen vacancies are [39]. So according to the Fig. 4 the content of oxygen vacancies varies with different ZnO films shows the following order: 3# > 2# > 4# > 1#.

The room temperature UV–Vis diffuse reflectance spectra of the ZnO films are displayed in Fig. 5. Film 3# exhibits a greatly enhanced absorption compare with other films.

In our study, the photocatalytic performance was evaluated by photodegradation of the well known organic azo-dye N,N,N′,N′-tetra ethylated rhodamine (RhB), a typical pollutant in the textile industry, under ultraviolet irradiation. The results of the RhB degradation used different ZnO photocatalysts are summarized in Fig. 6(a). Without any catalyst, only a slow decrease in the concentration of RhB was detected under UV irradiation. The photocatalytic activity depends on the morphology of ZnO films. The activity shows the following order: 3# > 2# > 4# > 1#. After 10 h of irradiation, the RhB in aqueous solution could be almost completely eliminated by the film 3#.

In order to monitor the photodegradation efficiency of ZnO films, we have done reusability study of the best sample (ZnO film 3#). The regenerated photocatalyst after the degradation experiments were washed and dried before used for further run. The inset

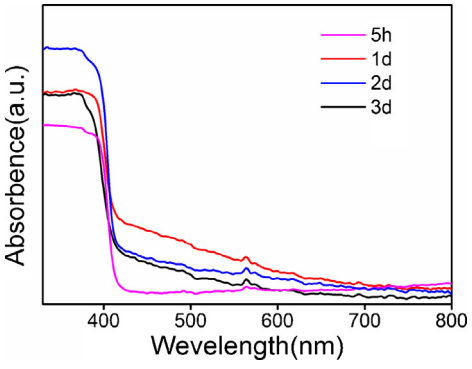

Fig. 5. The UV–Vis diffuse reflectance spectra for ZnO films after different deposition time.

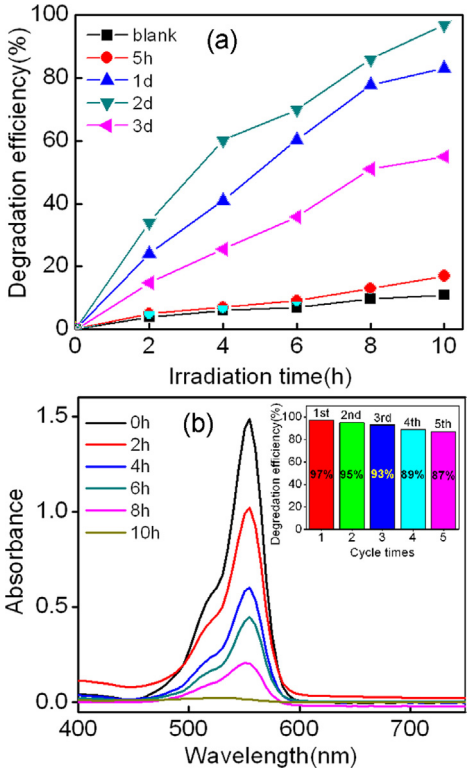

Fig. 6. (a) Degradation efficiency versus reaction time for ZnO films after different deposition times. (b) UV–visible absorbance spectra of dye solution with time over the best catalyst (ZnO film 3#). The inset image in (b) is the reusability of the best sample (ZnO film 3#).

image in Fig (b) represents the degradation efficiency of ZnO film 3# for 5 consecutive runs. Up to 5 runs, 87% photodegradation was noted, within 10 h.

The photocatalytic superiority of the film 3# over the other nanostructured ZnO can be attributed to their special structural features. Under UV irradiation, as long as photons enter into ZnO cages they will be reflected by the cage bars for many times before they escape from jails. The increase in reflect times in cages leads absorption of photons by ZnO cages. And that is to say film 3# can use solar energy much more efficiency than its counterpart. The function of capture photons by ZnO cages is similar to black body, a physics model, to a certain degree. Base on similar explanation, film 3# with ZnO cages on surface can also play the role of RhB molecules traps. Once RhB molecules enter into ZnO cages, they have more opportunity to contact surface of ZnO material than on other films. RhB molecules will react with hydroxyl radicals on the surface of ZnO more smoothly. So most of RhB molecules will be degraded completely before free diffused out of cages.

In addition, film 3# has the biggest content of oxygen vacancies among different ZnO films according to Fig. 4. Due to nonsaturable oxygen coordination, oxygen vacancies on the surface of ZnO will result in a distinct ability to absorb the oxygen species (such as O_2, OH^-) and target molecules through chemical/physical absorption [40]. Based on the theory, film 3# can adsorb more OH^- and H_2O in the solution condition of photodegradation. The excited electron are trapped by O_2 to form superoxide radical ion ($^{\bullet}O_2$), and the holes left in the valence band can react with adsorbed water (or surface hydroxyl) to form very reactive hydroxyl radicals ($^{\bullet}OH$), which subsequently attacks the adsorbed pollutant molecules to produce oxidized species and/or decomposed products can accelerate the photocatalysis reaction [41,42].

As stated above, good photocatalytic performance of film 3# is obtained. Obviously, the other nanostructured ZnO, lack the

above-mentioned structural advantage, and thus present relatively inferior photocatalytic activity in the photodegradation of RhB.

4. Conclusions

ZnO films with different morphology were obtained using hydrothermal method under different reaction times. ZnO cages exhibited superior ability on the photocatalytic degradation of RhB aqueous solution under UV radiation compared with other ZnO films. The higher photocatalytic activity of the ZnO cages results from the special morphology and the larger content of oxygen vacancy on the surface.

Acknowledgments

This work is supported by the National Programs for High Technology Research and Development of China (863) (Item No. 2013AA032202), National Natural Science Foundation of China (Grant Nos. 61178074 and 61378085), the National Youth Program Foundation of China (Grant No. 61308095), Program for the development of Science and Technology of Jilin province (Item No. 20130102004JC and 201115219).

References

[1] B.K. Sovacool, P. Parenteau, M.V. Ramana, S.V. Valentine, M.Z. Jacobson, M.A. Delucchi, M. Diesendorf, Comment on prevented mortality and greenhouse gas emissions from historical and projected nuclear power, Environ. Sci. Technol. 47 (2013) 6715–6717.
[2] J.C. Chow, J.G. Watson, Review of PM2.5 and PM10 apportionment for fossil fuel combustion and other sources by the chemical mass balance receptor model, Energy Fuels 16 (2002) 222–260.
[3] M.G. Zhou, Y.N. Liu, L.J. Wang, X.Y. Kuang, X.H. Xu, H.D. Kan, Particulate air pollution and mortality in a cohort of Chinese men, Environ. Pollut. 186 (2014) 1–6.
[4] H.B. He, B. Li, J.P. Dong, Y.Y. Lei, T.L. Wang, Q.W. Yu, Y.Q. Feng, Y.B. Sun, Mesostructured nanomagnetic polyhedral oligomeric silsesquioxanes (POSS) incorporated with dithiol organic anchors for multiple pollutants capturing in wastewater, ACS Appl. Mater. Inter. 5 (2013) 8058–8066.
[5] S. Lee, S.C. Yoon, S.W. Kim, Y.P. Kim, Y.S. Ghim, J.H. Kim, C.H. Kang, Y.J. Kim, L.S. Chang, S.J. Lee, Spectral dependency of light scattering/absorption and hygroscopicity of pollution and dust aerosols in Northeast Asia, Atmos. Environ. 50 (2012) 246–254.
[6] M. Usman, O. Tascone, P. Faure, K. Hannaf, Chemical oxidation of hexachlorocyclohexanes (HCHs) in contaminated soils, Sci. Total Environ. 476–477 (2014) 434–440.
[7] M. Gourmelon, M.P. Caprais, S. Mieszkin, R. Marti, N. Wéry, E. Jardé, M. Derrien, A. Jadas-Hécart, P.Y. Communal, A. Jaffrezic, A.M. Pourcher, Development of microbial and chemical MST tools to identify the origin of the faecal pollution in bathing and shellfish harvesting waters in France, Water Res. 44 (2010) 4812–4824.
[8] X.B. Chen, S.H. Shen, L.J. Guo, S.S. Mao, Semiconductor-based photocatalytic hydrogen generation, Chem. Rev. 110 (2010) 6503–6570.
[9] B. Dhal, H.N. Thatoi, N.N. Das, B.D. Pandey, Chemical and microbial remediation of hexavalent chromium from contaminated soil and mining/metallurgical solid waste: a review, J. Hazard. Mater. 250–251 (2013) 272–280.
[10] A. Fujishima, K. Honda, Electrochemical photolysis of water at a semiconductor electrode, Nature 238 (1972) 37–38.
[11] N. Liu, X.Y. Chen, J.L. Zhang, J.W. Schwank, A review on TiO_2-based nanotubes synthesized via hydrothermal method: formation mechanism, structure modification, and photocatalytic applications, Catal. Today 225 (2014) 34–51.
[12] V.R. de Mendonça, O.F. Lopes, R.P. Fregonesi, T.R. Giraldi, C. Ribeiro, TiO_2-SnO_2 heterostructures applied to dye photodegradation: The relationship between variables of synthesis and photocatalytic performance, Appl. Surf. Sci. 298 (2014) 182–191.
[13] M. Pudukudy, Z. Yaakob, Facile solid state synthesis of ZnO hexagonal nanogranules with excellent photocatalytic activity, Appl. Surf. Sci. 292 (2014) 520–530.
[14] F. Qin, R.M. Wang, G.F. Li, F. Tian, H.P. Zhao, R. Chen, Highly efficient photocatalytic reduction of Cr(VI) by bismuth hollow nanospheres, Catal. Commun. 42 (2013) 14–19.
[15] Y.Z. Wang, X.X. Xue, H. Yang, C. Luan, Preparation and characterization of Zn/Ce/SO_4^{2-}-doped titania nano-materials with antibacterial activity, Appl. Surf. Sci. 292 (2014) 608–614.
[16] J.H. Mo, Y.P. Zhang, Q.J. Xu, J.J. Lamson, R.Y. Zhao, Photocatalytic purification of volatile organic compounds in indoor air: A literature review, Atmos. Environ. 43 (2009) 2229–2246.
[17] D. Vildozo, C. Ferronato, M. Sleiman, J.M. Chovelon, Photocatalytic treatment of indoor air: optimization of 2-propanol removal using a response surface methodology (RSM), Appl. Catal. B: Environ. 94 (2010) 303–310.
[18] H. Hong, J. Shi, Y.N. Yang, Y. Zhang, J.W. Engle, R.J. Nickles, X.D. Wang, W.B. Cai, Cancer-targeted optical imaging with fluorescent zinc oxide nanowires, Nano Lett. 11 (2011) 3744–3750.
[19] J. Geng, G.H. Song, X.D. Jia, F.F. Cheng, J.J. Zhu, Fast one-step synthesis of biocompatible ZnO/Au nanocomposites with hollow doughnut-like and other controlled morphologies, J. Phys. Chem. C (116) (2012) 4517–4525.
[20] S.S. Xiao, L. Zhao, X.N. Leng, X.Y. Lang, J.S. Lian, Synthesis of amorphous TiO_2 modified ZnO nanorod film with enhanced photocatalytic properties, Appl. Surf. Sci. 299 (2014) 97–104.
[21] M. Pudukudy, Z. Yaakob, Hydrothermal synthesis of mesostructured ZnO micropyramids with enhanced photocatalytic performance, Superlattice. Microstruct. 63 (2013) 47–57.
[22] Z. Li, W. Shen, W. He, X. Zu, Effect of Fe-doped TiO_2 nanoparticle derived from modified hydrothermal process on the photocatalytic degradation performance on methylene blue, J. Hazard. Mater. 155 (2008) 590–594.
[23] J. Becker, K.R. Raghupathi, J.S. Pierre, D. Zhao, R.T. Koodali, Tuning of the crystallite and particle sizes of ZnO nanocrystalline materials in solvothermal synthesis and their photocatalytic activity for dye degradation, J. Phys. Chem. C 115 (2011) 13844–13850.
[24] M. Pudukudy, Z. Yaakob, Simple chemical synthesis of novel ZnO nanostructures: role of counter ions, Solid State Sci. 30 (2014) 78–88.
[25] M. Chekini, M.R. Mohammadizadeh, S.M. Vaez Allaei, Photocatalytic and superhydrophilicity properties of N-doped TiO_2 nanothin films, Appl. Surf. Sci. 257 (2011) 7179–7183.
[26] L. Rojas-Blanco, M.D. Urzúa, R. Ramírez-Bon, F.J. Espinoza Beltrán, Photocatalytic thin films containing TiO_2:N nanopowders obtained by the layer-by-layer self-assembling method, Appl. Surf. Sci. 258 (2012) 2103–2106.
[27] D.W. Lee, K.J. Yong, Partial conversion reaction of ZnO nanowires to ZnSe by a simple selenization method and their photocatalytic activities, Mater. Chem. Phys. 137 (2012) 194–199.
[28] W. Lee, M.C. Jeong, J.M. Myoung, Evolution of the morphology and optical properties of ZnO nanowires during catalyst-free growth by thermal evaporation, Nanotechnology 15 (2004) 1441–1445.
[29] S. Bayan, P. Chakraborty, Secondary ion mass spectrometry and photoluminescence study on microstructural characteristics of chemically synthesized ZnO nanowalls, Appl. Surf. Sci. 303 (2014) 233–240.
[30] A.B. Djurišić, W.C.H. Choy, V.A.L. Roy, Y.H. Leung, C.Y. Kwong, K.W. Cheah, T.K. Gundu Rao, W.K. Chan, H. Fei Lui, C. Surya, Photoluminescence and electron paramagnetic resonance of ZnO tetrapod structures, Adv. Funct. Mater. 14 (2004) 856–864.
[31] K. Vanheusden, C.H. Seager, W.L. Warren, D.R. Tallant, J. Voigt, Correlation between photoluminescence and oxygen vacancies in ZnO phosphors, Appl. Phys. Lett. 68 (1996) 403–405.
[32] A. van Dijken, E.A. Meulenkamp, D. Vanmaekelbergh, A. Meijerink, The kinetics of the radiative and nonradiative processes in nanocrystalline ZnO particles upon photoexcitation, J. Phys. Chem. B 104 (2000) 1715–1723.
[33] B.X. Lin, Z.X. Fu, Y.B. Jia, Green luminescent center in undoped zinc oxide films deposited on silicon substrates, Appl. Phys. Lett. 79 (2001) 943–945.
[34] Q.X. Zhao, P. Klason, M. Willander, H.M. Zhong, W. Lu, J.H. Yang, Deep-level emissions influenced by O and Zn implantations in ZnO, Appl. Phys. Lett. 87 (2005) 211912.
[35] S.A. Studenikin, N. Golego, M. Cocivera, Fabrication of green and orange photoluminescent, undoped ZnO films using spray pyrolysis, J. Appl. Phys. 84 (1998) 2287–2294.
[36] A.B. Djurišić, Y.H. Leung, K.H. Tam, L. Ding, W.K. Ge, H.Y. Chen, S. Gwo, Green, yellow, and orange defect emission from ZnO nanostructures: Influence of excitation wavelength, Appl. Phys. Lett. 88 (2006) 103107.
[37] S. Monticone, R. Tufeu, A.V., Complex nature of the UV and visible fluorescence of colloidal ZnO nanoparticles, J. Phys. Chem. B 102 (1998) 2854–2861.
[38] L.L. Wu, Y.S. Wu, X.R. Pan, F.Y. Kong, Synthesis of ZnO nanorod and the annealing effect on its photoluminescence property, Opt. Mater. 28 (2006) 418–422.
[39] K. Vanheusden, W.L. Warren, C.H. Seager, D.R. Tallant, J.A. Voigt, B.E. Gnade, Mechanisms behind green photoluminescence in ZnO phosphor powders, J. Appl. Phys. 79 (1996) 7983–7990.
[40] E.S. Jang, J.H. Won, S.J. Hwang, J.H. Choy, Fine tuning of the face orientation of ZnO crystals to optimize their photocatalytic activity, Adv. Mater. 18 (2006) 3309–3312.
[41] Q.J. Xiang, J.G. Yu, P.K. Wong, Quantitative characterization of hydroxyl radicals produced by various photocatalysts, J. Colloid Interface Sci. 357 (2011) 163–167.
[42] Q.J. Xiang, J.G. Yu, W.G. Wang, M. Jaronie, Nitrogen self-doped nanosized TiO_2 sheets with exposed {0 0 1} facets for enhanced visible-light photocatalytic activity, Chem. Commun. 47 (2011) 6906–6908.